Understanding the Electronic Structure of IrO_2 Using Hard-X-ray Photoelectron Spectroscopy and Density-Functional Theory

J. M. Kahk,[1] C. G. Poll,[1] F. E. Oropeza,[1] J. M. Ablett,[2] D. Céolin,[2] J-P. Rueff,[2] S. Agrestini,[3] Y. Utsumi,[3] K. D. Tsuei,[4] Y. F. Liao,[4] F. Borgatti,[5] G. Panaccione,[6] A. Regoutz,[7] R. G. Egdell,[7] B. J. Morgan,[8] D. O. Scanlon,[9,10] and D. J. Payne[1,*]

[1]*Department of Materials, Imperial College London, Exhibition Road, London SW7 2AZ, United Kingdom*
[2]*Synchrotron SOLEIL, L'Orme des Merisiers, BP 48 Saint-Aubin, 91192 Gif-sur-Yvette, France*
[3]*Max Planck Institute for Chemical Physics of Solids, Nöthnitzerstr. 40, 01187 Dresden, Germany*
[4]*National Synchrotron Radiation Research Center, 101 Hsin-Ann Road, Hsinchu 30077, Taiwan*
[5]*Consiglio Nazionale delle Ricerche, Istituto per lo Studio dei Materiali Nanostrutturati (CNR-ISMN), via P. Gobetti n.101, I-40129 Bologna, Italy*
[6]*Istituto Officina dei Materiali (IOM)-CNR, Laboratorio TASC, in Area Science Park, S.S.14, Km 163.5, I-34149 Trieste, Italy*
[7]*Department of Chemistry, University of Oxford, Chemistry Research Laboratory, 12 Mansfield Road, Oxford OX1 3TA, United Kingdom*
[8]*Department of Materials, University of Oxford, Parks Road, Oxford OX1 3PH, United Kingdom*
[9]*University College London, Kathleen Lonsdale Materials Chemistry, Department of Chemistry, 20 Gordon Street, London WC1H 0AJ, United Kingdom*
[10]*Diamond Light Source Ltd., Diamond House, Harwell Science and Innovation Campus, Didcot, Oxfordshire OX11 0DE, United Kingdom*

(Received 13 September 2013; revised manuscript received 25 November 2013; published 17 March 2014)

The electronic structure of IrO_2 has been investigated using hard x-ray photoelectron spectroscopy and density-functional theory. Excellent agreement is observed between theory and experiment. We show that the electronic structure of IrO_2 involves crystal field splitting of the iridium 5*d* orbitals in a distorted octahedral field. The behavior of IrO_2 closely follows the theoretical predictions of Goodenough for conductive rutile-structured oxides [J. B. Goodenough, J. Solid State Chem. **3**, 490 (1971)]. Strong satellites associated with the core lines are ascribed to final state screening effects. A simple plasmon model for the satellites applicable to many other metallic oxides appears to be not valid for IrO_2.

DOI: 10.1103/PhysRevLett.112.117601 PACS numbers: 79.60.-i, 71.20.-b, 71.10.-w

A series of iridium-containing ternary oxides (iridates) have attracted increasing attention due to their diverse electronic properties. Some iridates such as $BaIrO_3$ and $Bi_2Ir_2O_7$, are metallic [1,2] while others exhibit an exotic range of electronic properties including Mott insulators [3], topological insulators [4,5], Weyl semimetals [6], and axion insulators [6]. Many undergo a metal-insulator transition when cooled [4,7], and some show highly unusual magnetic properties at low temperatures [8]. The origins of such diversity lie within the complex behavior of the Ir 5*d* electrons: as the energy scales of crystal-field splitting, electron-electron repulsion, spin-orbit coupling, and various spin-exchange interactions approach each other, small changes in structure can lead to vastly different observable properties.

The aforementioned studies have inspired a recent revival of interest in the fundamental properties of the simple binary iridium oxide IrO_2. Miao *et al.* [9] have used density-functional theory calculations to investigate the categorical stability of the Ir^{4+} oxidation state in binary iridium–oxygen compounds, while Clancy *et al.* [10] and Hirata *et al.* [11] performed x-ray absorption spectroscopy (XAS) and anisotropic tensor of susceptibility (ATS) scattering measurements, respectively, on a range of iridates and ruthenates, and observed a surprisingly large spin-orbit splitting in the IrO_2 valence band. However, there are still important aspects of the electronic structure of IrO_2 that deserve further attention. In particular, definitive answers are required for the following two fundamental questions: which physical mechanisms, if any, dominate the band structure of IrO_2, and why is IrO_2 a metal, while several seemingly similar iridates are not? Our interest in IrO_2 is further fueled by its great technological importance, with current or potential applications in areas ranging from optical information storage [12], electrochromic devices [13], and semiconductor electronics [14] to gas sensing [15], *p*H measurement [16], catalysis [17], and spintronics [18].

In this Letter, we present high-resolution hard x-ray photoelectron spectroscopy (HAXPES) measurements of IrO_2, complemented by theoretical band-structure calculations within the framework of density-functional theory (DFT). These results lead to a detailed understanding of the electronic structure of IrO_2, particularly the nature of electronic states near the Fermi level. Additionally, IrO_2 core-level photoelectron spectra of IrO_2 will be presented, and the interpretation of the core-level line shapes will be discussed briefly.

The photoemission measurements were performed on a ceramic pellet of IrO_2 (99.9%, Sigma Aldrich), pressed

at 5 tonnes and sintered at 800 °C for 5 hours in air. After firing, phase purity was confirmed using x-ray diffraction (see Supplemental Material [19]). HAXPES measurements were conducted at 6.5 keV using the photoemission setup of the Max Planck Institute for Chemical Physics of Solids on the Taiwan beamline BL12 XU at the Spring-8 synchrotron radiation facility (Japan), and additionally at various excitation energies on the GALAXIES beamline at the Soleil synchrotron. All measurements were performed in normal emission. All calculations were performed using the VASP package [20,21], in which the valence electronic states are expanded within a plane-wave basis. The valence-core interactions were described using the projector augmented wave (PAW) approach [22], and cores of [He] for oxygen, and [Xe] for iridium, were used. The Perdew-Burke-Ernzerhof functional revised for solids (PBEsol) exchange-correlation functional [23] and a cutoff of 750 eV were used for the all calculations, with the Brillouin zone sampled using a $6 \times 6 \times 4$ Monkhorst Pack grid. Calculations were deemed to have converged when the forces on all the atoms were less than 0.01 eV Å^{-1}, and the calculations were performed both with and without spin-orbit-coupling.

The HAXPES spectrum and DFT calculation of the valence band of IrO_2 are shown in Fig. 1(a) and the Ir $4f$ and Ir $5p$ core levels of IrO_2 are shown in Fig. 1(b). The measured valence band spectrum agrees well with previous XPS measurements [24–27], but shows a significantly greater level of detail due to improved energy resolution. In addition the cross-section weighted total density of states (tDOS) DFT calculation [Fig. 1(a) (lower)] shows excellent agreement with the experimental spectrum. The features in the valence band denoted II, III, and IV correspond to Ir-O π antibonding, π bonding, and σ bonding orbitals, respectively. One has to keep in mind that the photoionization cross section of the Ir $5d$ electrons is significantly greater than that of the O $2p$ electrons at 6.5 keV photon energy [28], and the measured spectrum is dominated by the iridium $5d$ orbitals.

What is not clear from the elementary analysis presented is the origin of the small feature (labeled I) close to the Fermi level. It is first worth noting that a similar shoulder has been observed in theoretical densities of states for iridates, such as $CaIrO_3$ [29], for which it was attributed as arising from spin-orbit splitting of the Ir $5d$ t_{2g} band into $j = \frac{3}{2}$ and $j = \frac{1}{2}$ subbands, occupied by four electrons and one electron, respectively. Spin-orbit coupling has also been invoked to explain the shoulder in IrO_2 [24], but previous calculations [9,30–32] suggest that a simpler explanation is provided by orbital-overlap effects made possible by the strong deviation from perfect octahedral symmetry in rutile IrO_2. Total and partial density of states with and without spin-orbit coupling (SOC) are shown in Fig. 2. It is immediately apparent that the low binding energy feature (I) is present even when effects of valence-electron spin-orbit coupling are omitted from the calculation.

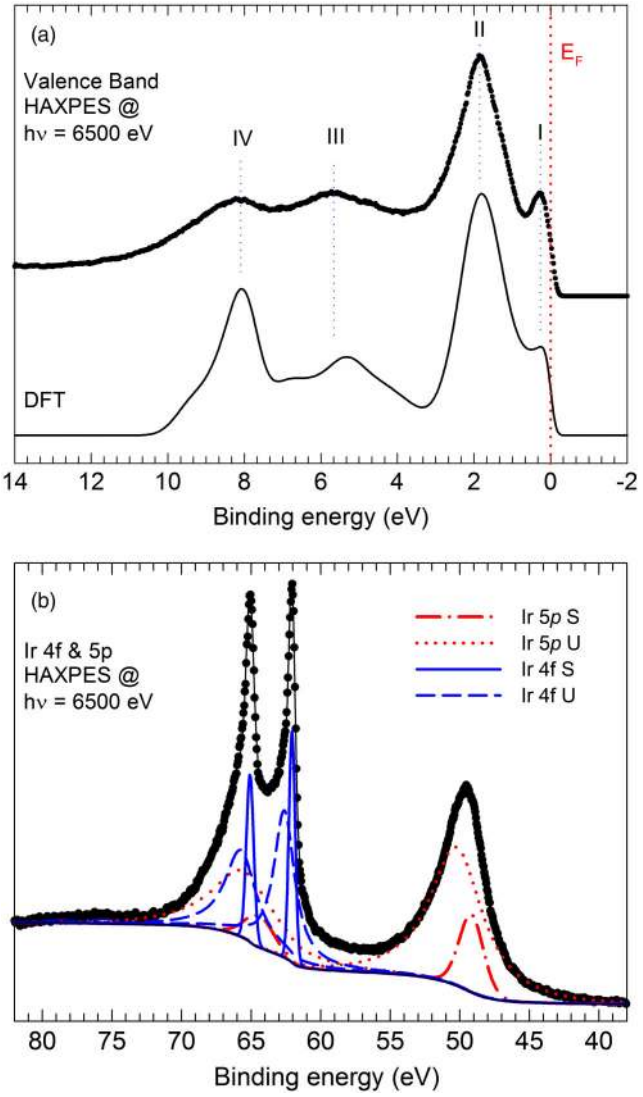

FIG. 1 (color online). (a) HAXPES spectrum of the valence band of IrO_2 measured at a photon energy of 6571.65 eV and cross-section weighted DFT calculation showing partial and total densities of states. (b) HAXPES spectrum of the Ir f and Ir $5p$ core levels. The screened (S) and unscreened (U) components for Ir $4f$ (blue) and Ir $5p$ (red) are shown. Note: The Ir $5p_{\frac{1}{2}}$ component lies within the structure of the Ir f spin-orbit doublet.

To further discern the nature of the electronic states near the Fermi level, the contributions of the individual Ir d orbitals to the overall density of states were calculated by projecting on to $l = 2$ spherical harmonics within the Ir PAW radii (Fig. 3). It is important to note that for our calculations the coordinate system shown in Fig. 4(a) is based on a $\sqrt{2} \times \sqrt{2}$ supercell in accordance to the local geometry of the iridium atom and does not match the overall unit cell. This allows us to discuss our results in terms of the Goodenough model for conductive rutile oxides [33,34] [Fig. 4(b)].

From Fig. 3, it can be seen that the degeneracy of the five iridium d orbitals has been completely lifted by the crystal field of D_{2h} coordination symmetry. Nevertheless, it is still

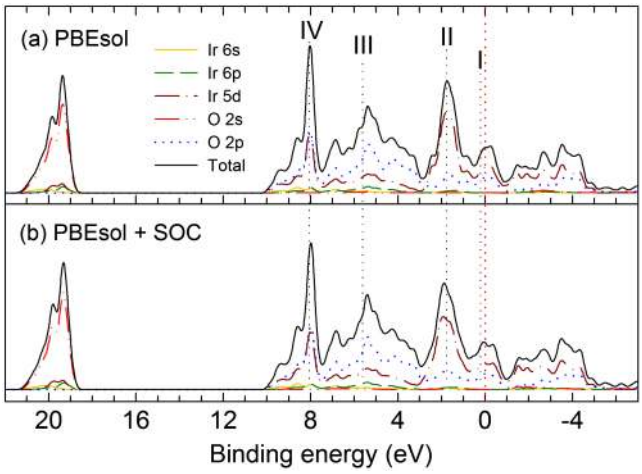

FIG. 2 (color online). (a) Density functional theory calculations of the total and partial density of states for IrO_2. (b) Total and partial density of states for IrO_2 including spin-orbit coupling (SOC).

possible to identify two of the Ir d orbitals (d_{z^2} and d_{xy}) as being primarily σ antibonding in nature (e_g-like), whereas the other three are primarily π antibonding (t_{2g}-like). We see that the $d_{x^2-y^2}$ orbital gives a narrow band $\sim$1 eV below E_F, whereas the d_{yz} and d_{xz} bands are much broader and are responsible for almost all of the electron density at the Fermi level. This can be understood in terms of the connectivity of the IrO_6 octahedra in the rutile structure. Along the c axis, neighbouring octahedra share edges and the t_{2g}-like orbitals differ in their relative orientation to the plane formed by these shared edges. One of the t_{2g} orbitals lies within the plane formed by the shared edges and is denoted $t_{\|}$ because it has σ symmetry with respect to the axis defined by the chain of octahedra. The $t_{\|}$ orbitals show little mixing with the O $2p$ states. The other two t_{2g} orbitals lie perpendicular to the octahedra-edge-sharing plane and are denoted $t_{\perp}$. It is these orbitals that contribute almost all of the density of states at the Fermi level.

Our detailed understanding of the nature of the three t_{2g} orbitals in IrO_2 provides an explanation for why valence electron spin-orbit coupling does not lead to insulating behavior in this material. For insulating iridates the ground state can, to a first approximation, be described as a $j_{\text{eff}} = \frac{1}{2}$ spin-orbit Mott insulator [29,35]. In this type of a material, the d orbitals of t_{2g} symmetry largely retain their atomic orbital-like degeneracy, and behave as a set with an orbital angular momentum of $l = 1$. Spin-orbit coupling leads to the formation of a fully occupied $j = \frac{3}{2}$ band and a half-empty $j = \frac{1}{2}$ band, separated by a direct or indirect band gap. Provided the $j = \frac{1}{2}$ band is sufficiently narrow, even moderate electron-electron repulsion can drive the system into a Mott insulating state. While it has been pointed out that as a quantitative model the concept of $j_{\text{eff}} = \frac{1}{2}$ physics is no longer strictly valid under even small deviations from octahedral symmetry [36], as a qualitative model it seems to have a certain degree of tolerance for minor distortions.

First, in the case of IrO_2, we note that one of the three t_{2g} orbitals has fundamentally different bonding properties to the other two, which makes the application of any model

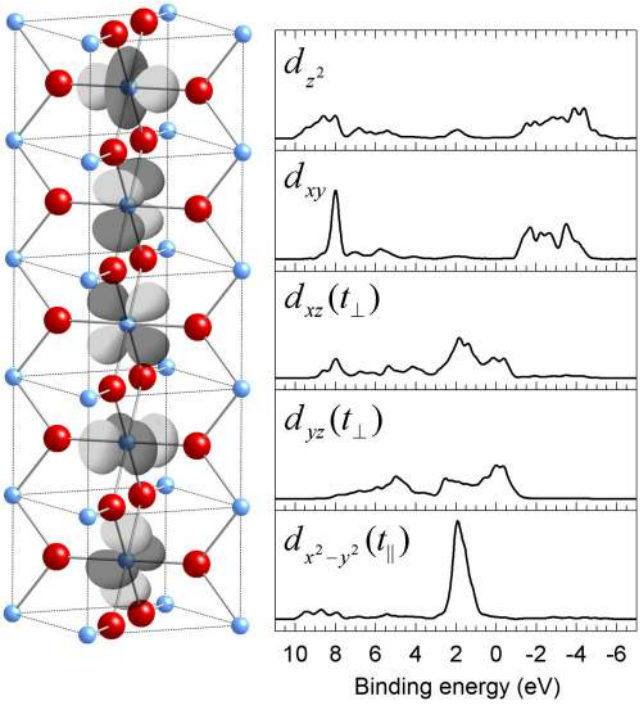

FIG. 3 (color online). Left: a stack of five unit cells showing the IrO_2 rutile structure in the revised coordinate system. Also shown are the five Ir $5d$ orbitals highlighting their orientation relative to the unit cell coordinates. Right: Ir $5d$ partial densities of states projected onto their representative atomic orbitals.

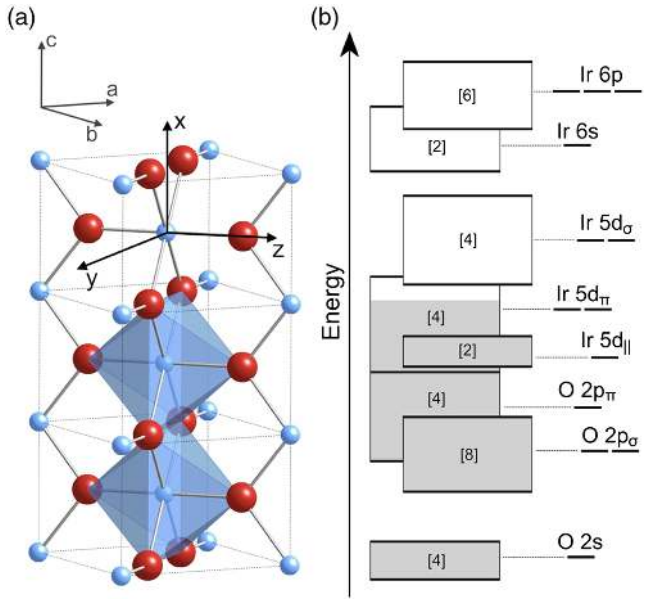

FIG. 4 (color online). (a) The rutile crystal structure of the iridium-centred unit cell with the x, y, and z coordinates defined. (b) Schematic description (Goodenough model [33]) of the electronic structure of IrO_2.

that relies on the three behaving as a "set" with $l = 1$ rather doubtful. Second, we observe that the bands in IrO_2 are not narrow, with the total width of the valence band exceeding 10 eV, and that of the t_{2g} manifold around 4 eV. Both values are greater than calculated bandwidths for the insulating iridate $CaIrO_3$ [29]. Third, we see that both the orthogonal Ir $5d$ d_{xz} and d_{yz} ($t_\perp$) orbitals contribute strongly to the density of states at the Fermi level, and are therefore similarly responsible for the conduction properties of the material.

It is these three observations that allow us to state that in IrO_2 the effects of crystal-field splitting and effective orbital overlap completely dominate the effects of valence electron spin-orbit coupling and electron-electron repulsion, giving rise to the metallic behavior. While recognizing that strong spin-orbit coupling interactions for the Ir $5d$ electrons must exist in IrO_2 [10,11], they do not seem to be responsible for any of the major features of the band structure. Based on these results we also predict that the metallicity of IrO_2 should be quite robust with respect to external influences such as doping or nonstoichiometry, but effects that change the relative nature of the t_{2g} orbitals, such as epitaxial strain along the direction of the c axis, could possibly lead to a marked change in the observed behavior.

The metallic nature of IrO_2 also manifests itself in the HAXPES core levels of IrO_2, which exhibit a distinctly asymmetric shape. In Fig. 1(b) the Ir $4f$ and $5p$ region of the HAXPES spectrum is displayed. This region was chosen for comparison with previously published core-level XPS studies of IrO_2, which primarily focus on the interpretation of the Ir $4f$ peak shape [26,27,32,37–49]. The most striking feature of the core levels in IrO_2 is that all of the peaks show a strong asymmetry. The most tenable explanation for this is formulated in terms of final-state effects during the photoemission process. The phenomenon of conduction electron screening in the core-level spectroscopy of metallic conductors has been well established for over 30 years, and is applicable for a wide range of metal oxides [50–53].

Two different models have been used to explain the nature of core satellites in narrow band metals. In the Kotani model [54] generation of the core hole in the photoemission process switches on a local Coloumb interaction with the valence states contributing to the conduction band. If this interaction exceeds the occupied conduction band width, the potential will create a localized state on the ionized atom. Two possible final states are now accessible to the system: the low binding energy peak corresponds to the localized state being filled (core hole is screened) and the high binding energy peak is a result of the state remaining empty (core hole is unscreened). This model has been successfully applied to a range of narrow-band conductive metal oxides [50–53]. The second model treats the core line as a low binding energy "main" peak and the high binding energy peak as an unusually strong plasmon satellite, broadened by conduction electron scattering. It has been suggested by theory that the intensity of the high binding energy satellite (in low electron density metals) should increase in intensity with decreasing electron density ($n^{-(1/3)}$) [55]. It has also been shown in a number of metallic oxide systems that the satellite energies are close to plasmon energies measured by electron energy loss spectroscopy or infrared reflectance spectroscopy [50,56].

It was clear upon peak-fitting the Ir $4f$ core level that it will not fit with a single Voigt component or a Fano-type line shape for metallic systems. The best fits were obtained by using two Voigt components, with constraints applied to the relative intensities of the two halves of each spin-orbit doublet, and the relative positions of the main peaks. Good fits were obtained for various core levels (peak fits of core levels measured at different excitation energies are presented in the Supplemental Material [19]). Interestingly, we found that constraining the separation between screened and unscreened components of each individual core line to the same value leads to a rapid deterioration in the quality of the peak fits. This suggests that the simple plasmon excitation model may not be appropriate for IrO_2. It therefore remains a significant challenge to theorists to reconcile these two apparently distinct models. It should, however, be noted that only a handful of publications dealing with core-level XPS of IrO_2 have considered the role of final state screening [26,41,45,47]. On the other hand, it has been repeatedly but incorrectly argued that complex line shapes must imply different oxidation states in the initial state [39,40]. Implausible surface phases containing Ir^{6+} have been invoked, and it has even been postulated that commercial IrO_2 samples contain some Ir_2O_3, even though no such bulk phase is known to exist [26,57]. Surface sensitivity is much reduced in HAXPES and the present observation of complex line shapes at an excitation energy above 6 keV provides further evidence in favor of the intrinsic origin of the asymmetry in IrO_2. As a last remark, we note that similar intrinsically asymmetric core line shapes ought to be expected in HAXPES or XPS studies of other metallic oxides of iridium, but not the insulating iridates. As such, core level photoelectron spectroscopy could be a useful tool for studying the metal-insulator transition in iridates, and conversely, iridates could provide a suitable testing ground for probing the specifics of the influence of the conduction electrons on the core level XPS signature. One example of the use of core level XPS for monitoring the metal insulator transition in a ternary iridium sulphate has already been published [58].

In conclusion, we have used hard x-ray photoelectron spectroscopy and density-functional theory calculations to study the electronic structure of iridium oxide. An excellent level of agreement between theory and experiment was observed. We have examined the decomposition of the valence band density of states into individual iridium $5d$ orbitals, and shown that IrO_2 conforms well to the

Goodenough model for conductive rutile oxides [33]. The vastly different bonding properties of the Ir $5d$ $t_{\|}$ and $t_{\perp}$ orbitals in conjunction with the large bandwidths of the Ir d bands explain why a spin-orbit Mott insulating state is not observed in IrO_2. Additionally, we have presented core-level photoelectron spectra of IrO_2, and have shown that the observed line shapes are consistent with the formalism of screened and unscreened final states, which has previously been successfully applied to a range of conductive metal oxides.

D. J. P. acknowledges support from the Royal Society (UF100105). J. M. K. acknowledges support from EPSRC for a Doctoral Prize Studentship. D. J. P. and D. O. S. acknowledge the support of the Materials Design Network. We gratefully acknowledge the NSRRC and the SPring-8 staff for providing us with beamtime. The German part of the research is partially supported by the Deutsche Forschungsgemeinschaft through SFB 608 and FOR 1346. The computational work presented here made use of the IRIDIS cluster provided by the EPSRC-funded Centre for Innovation (EP/K000144/1 and EP/K000136/1), and the HECToR supercomputer through our membership of the UK's HPC Materials Chemistry Consortium, which is funded by EPSRC Grant No. EP/F067496. D. O. S. is grateful to the Ramsay Memorial Trust and UCL for support received from a Ramsay Fellowship. J. M. K and C. G. P. contributed equally to this work.

*To whom all correspondence should be addressed.
d.payne@imperial.ac.uk

[1] Y. S. Lee, S. J. Moon, S. C. Riggs, M. C. Shapiro, I. R. Fisher, B. W. Fulfer, J. Y. Chan, A. F. Kemper, and D. N. Basov, Phys. Rev. B **87**, 195143 (2013).
[2] J. Zhao, L. Yang, Y. Yu, F. Li, R. Yu, and C. Jin, Inorg. Chem. **48**, 4290 (2009).
[3] H. H. Gretarsson, J. P. Clancy, X. Liu, J. P. Hill, E. Bozin, Y. Singh, S. Manni, P. Gegenwart, J. Kim, A. H. Said *et al.*, Phys. Rev. Lett. **110**, 076402 (2013).
[4] B. J. Yang and Y. B. Kim, Phys. Rev. B **82**, 085111 (2010).
[5] M. Kargarian, J. Wen, and G. A. Fiete, Phys. Rev. B **83**, 165112 (2011).
[6] X. Wan, A. M. Turner, A. Vishwanath, and S. Y. Savrasov, Phys. Rev. B **83**, 205101 (2011).
[7] K. Matsuhira, M. Wakeshima, R. Nakanishi, T. Yamada, A. Nakamura, W. Kawano, S. Takagi, and Y. Hinatsu, J. Phys. Soc. Jpn. **76**, 043706 (2007).
[8] S. M. Disseler, S. R. Giblin, C. Dhital, K. C. Lukas, S. D. Wilson, and M. J. Graf, Phys. Rev. B **87**, 060403(R) (2013).
[9] M.-S. Miao and R. Seshadri, J. Phys. Condens. Matter **24**, 215503 (2012).
[10] J. P. Clancy, N. Chen, C. Y. Kim, W. F. Chen, K. W. Plumb, B. C. Jeon, T. W. Noh, and Y.-J. Kim, Phys. Rev. B **86**, 195131 (2012).
[11] Y. Hirata, K. Ohgushi, J.-i. Yamaura, H. Ohsumi, S. Takeshita, M. Takata, and T.-h. Arima, Phys. Rev. B **87**, 161111(R) (2013).
[12] S. Hackwood, G. Beni, M. A. Bosch, K. Kang, L. M. Schiavone, and J. L. Shay, Phys. Rev. B **26**, 7073 (1982).
[13] C. G. Granqvist, E. Avendano, and A. Azens, Thin Solid Films **442**, 201 (2003).
[14] S. W. Kim, S. H. Kwon, D. K. Kwak, and S.-W. Kang, J. Appl. Phys. **103**, 023517 (2008).
[15] G. Shi, M. Luo, J. Xue, Y. Xian, L. Jin, and J. Y. Jin, Talanta **55**, 241 (2001).
[16] P. Kurzweil, Sensors **9**, 4955 (2009).
[17] S. D. Tilley, M. Cornuz, K. Sivula, and M. Grätzel, Angew. Chem., Int. Ed. **49**, 6405 (2010).
[18] K. Fujiwara, Y. Fukuma, J. Matsuno, H. Idzuchi, Y. Niimi, Y. Otani, and H. Takagi, Nat. Commun. **4**, 2893 (2013).
[19] See Supplemental Material at http://link.aps.org/supplemental/10.1103/PhysRevLett.112.117601 for an x-ray diffraction pattern of iridium dioxide and additional peak fits of measured core levels (Ir $4p$, $4f$ and Ir $5p$) as well as tabulated values of core level component binding energy, peak area, full width half maximum and Gaussian/Lorentzian ratios.
[20] G. Kresse and J. Hafner, Phys. Rev. B **49**, 14251 (1994).
[21] G. Kresse and J. Furthmüller, Comput. Mater. Sci. **6**, 15 (1996).
[22] P. E. Blöchl, Phys. Rev. B **50**, 17953 (1994).
[23] J. P. Perdew, A. Ruzsinszky, G. I. Csonka, O. A. Vydrov, G. E. Scuseria, L. A. Constantin, X. Zhou, and K. Burke, Phys. Rev. Lett. **100**, 136406 (2008).
[24] J. Riga, C. Tenret-Noel, J. J. Pireaux, R. Caudano, J. J. Verbist, and Y. Gobillon, Phys. Scr. **16**, 351 (1977).
[25] R. R. Daniels, G. Margaritondo, C.-A. Georg, and F. Levy, Phys. Rev. B **29**, 1813 (1984).
[26] G. K. Wertheim and H. J. Guggenheim, Phys. Rev. B **22**, 4680 (1980).
[27] R. Kötz, H. Neff, and J. Stucki, J. Electrochem. Soc. **131**, 72 (1984).
[28] J. H. Scofield, "Theoretical Photoionization Cross-Sections from 1 to 1500 keV," Lawrence Livermore Laboratory, Technical Report No. UCRL 51326, 1973.
[29] A. Subedi, Phys. Rev. B **85**, 020408(R) (2012).
[30] L. F. Mattheiss, Phys. Rev. B **13**, 2433 (1976).
[31] J. S. de Almeida and R. Ahuja, Phys. Rev. B **73**, 165102 (2006).
[32] J. Xu, M. Wang, G. Liu, J. Li, and X. Wang, Electrochim. Acta **56**, 10223 (2011).
[33] J. B. Goodenough, J. Solid State Chem. **3**, 490 (1971).
[34] F. H. J. A. Gulino, T S. Parker, and R. G. Egdell, J. Chem. Soc., Faraday Trans. **92**, 2137 (1996).
[35] Y. Okada, D. Walkup, H. Lin, C. Dhital, T. R. Chang, S. Khadka, W. Zhou, H. T. Jeng, M. Paranjape, A. Bansil *et al.*, Nat. Mater. **12**, 707 (2013).
[36] X. Liu, V. M. Katukuri, L. Hozoi, W.-G. Yin, M. P. M. Dean, M. H. Upton, J. Kim, D. Casa, A. Said, T. Gog *et al.*, Phys. Rev. Lett. **109**, 157401 (2012).
[37] R. Ktz, H. Lewerenz, P. Brüesch, and S. Stucki, J. Electroanal. Chem. **150**, 209 (1983).
[38] M. Hara, K. Asami, K. Hashimoto, and T. Masumoto, Electrochim. Acta **28**, 1073 (1983).
[39] H. Y. Hall and P. M. A. Sherwood, J. Chem. Soc., Faraday Trans. 1 **80**, 135 (1984).
[40] J. Augustynski, M. Koudelka, J. Sanchez, and B. E. Conway, J. Electroanal. Chem. **160**, 233 (1984).

[41] I. M. Kodintsev, S. Trasatti, M. Rubel, A. Wieckowski, and N. Kaufher, Langmuir **8**, 283 (1992).
[42] V. A. Alves, L. A. da Silva, S. C. de Castro, and J. F. C. Boodts, J. Chem. Soc., Faraday Trans. **94**, 711 (1998).
[43] L. da Silva, V. Alves, S. de Castro, and J. Boodts, Colloids Surf. A **170**, 119 (2000).
[44] R.-S. Chen, Y.-S. Huang, Y.-M. Liang, D.-S. Tsai, Y. Chi, and J.-J. Kai, J. Mater. Chem. **13**, 2525 (2003).
[45] Y. Liu, H. Masumoto, and T. Goto, Mater. Trans. **45**, 900 (2004).
[46] A. Korotcov, Y.-S. Huang, D.-S. Tsai, and K.-K. Tiong, J. Phys. Condens. Matter **18**, 1121 (2006).
[47] W.-H. Chung, C.-C. Wang, D.-S. Tsai, J.-C. Jiang, Y.-C. Cheng, L.-J. Fan, Y.-W. Yang, and Y.-S. Huang, Surf. Sci. **604**, 118 (2010).
[48] R. G. Haverkamp, A. T. Marshall, and B. C. C. Cowie, Surf. Interface Anal. **43**, 847 (2011).
[49] M. Li, Y. B. Wang, X. Zhang, Q. H. Li, Q. Liu, Y. Cheng, Y. Zheng, T. F. Xi, and S. C. Wei, Mater. Sci. Eng., C **33**, 15 (2013).
[50] D. J. Payne, R. G. Egdell, W. Hao, J. S. Foord, A. Walsh, and G. W. Watson, Chem. Phys. Lett. **411**, 181 (2005).
[51] C. Körber, V. Krishnakumar, A. Klein, , G. Panaccione, P. Torelli, A. Walsh, J. L. F. Da Silva, S. H. Wei, R. G. Egdell, and D. J. Payne, Phys. Rev. B **81**, 165207 (2010).
[52] J. N. Chazalviel, M. Campagna, G. K. Wertheim, and H. R. Shanks, Phys. Rev. B **16**, 697 (1977).
[53] D. O. Scanlon, G. W. Watson, D. J. Payne, G. R. Atkinson, R. G. Egdell, and D. S. L. Law, J. Phys. Chem. C **114**, 4636 (2010).
[54] A. Kotani, J. Electron Spectrosc. Relat. Phenom. **78**, 7 (1996).
[55] D. C. Langreth, in *Collective Properties of Physical Systems*, edited by B. Lundqvist (Academic press, New York, 1973), pp. 210–222.
[56] A. Bourlange, D. J. Payne, R. G. Palgrave, H. Zhang, J. S. Foord, R. G. Egdell, R. M. J. Jacobs, T. D. Veal, P. D. C. King, and C. F. McConville, J. Appl. Phys. **106**, 013703 (2009).
[57] M.-S. Miao and R. Seshadri, J. Phys. Condens. Matter **24**, 215503 (2012).
[58] K. Takubo, S. Hirata, J.-Y. Son, J. W. Quilty, T. Mizokawa, N. Matsumoto, and S. Nagata, Phys. Rev. Lett. **95**, 246401 (2005).